Computational and Experimental Studies of Microvascular Void Features for Passive-Adaptation of Structural Panel Dynamic Performance

Undergraduate Honors Thesis

By

Nicholas Sears

Honors Undergraduate Program in Mechanical Engineering

The Ohio State University

May 2017

Thesis Committee:

Ryan L. Harne, Advisor

Jason T. Dreyer

ABSTRACT

The performance, integrity, and safety of built-up structural systems are critical to their effective employment in diverse aerospace, automotive, civil, and marine engineering applications. In conflict with these goals, harmonic or random excitations of structural panels, which are common operating conditions for such systems, lead to oscillations at the modes of vibration occurring at the natural frequencies. The result is large amplitude vibrations that contribute directly to fatigue concerns, performance degradation, and ultimately failure. While many studies have considered active or passive damping treatments for structural control, these approaches exert little authority to tailor the frequency sensitivities central to the concern. To provide a more authoritative means to adapt the spectral properties of structural panels for advanced performance and safety, this research explores a new idea of designing the static and dynamic mass distribution of panels through embedded microvascular voids. Finite element model and experimental investigations study how removing mass in the form of microscale voids influences the global vibration modes and frequency sensitivities of structural panels. Through parameter studies, the relationships among void shape, size, number, and location are determined to serve as a guide for their use in subsequent dynamic mass distribution investigations. This research enables next-stage efforts that will characterize opportunities for real-time adaptation of the dynamic performance via fluid-filled microvascular channels that interface the microscale voids.

ACKNOWLEDGEMENTS

I would like to thank my advisor, Professor Ryan Harne, for the incredible amount of hard work and dedication he lends me and my fellow researchers in the pursuit of our academic and research success.

I would also like to thank Professor Jason Dreyer for the great insight, advice, and amount of time he makes available for me on a regular basis, as well as his willingness to help as the thesis committee member to my project.

All related experiments in this research are conducted in the Laboratory of Sound and Vibration Research (LSVR) that is directed by Dr. Harne.

TABLE OF CONTENTS

LIST OF FIGURES

LIST OF TABLES

1 INTRODUCTION

1.1 Background

Harmonic or random excitations of structures can lead to large-amplitude oscillations at the modes of vibration, which are significantly magnified when the structures are driven at their natural frequencies, or resonances. In gas turbines, for instance, the vibration response of the system under dynamic loading has been seen to become 1000 times its normal response when driven at resonance. This results in the failure of sensitive devices, or worse, failure of the entire system [1]. Furthermore, in the compressor blades of such gas turbines, it was found that oscillation at the lowest order natural frequency modes were the primary reason for fatigue fractures [2]. Damage to structures during earthquakes is also primarily a result of lower frequency excitations where large amplitude oscillations are experienced [3]. Therefore, the need to avoid such resonant operating conditions pertains to multiple concerns, including structure safety, performance, and integrity. One particular area of interest is in the vibration control of aircraft because vibrations at resonance are particularly dangerous, especially considering the severity of consequences in the event of failure. In fact, over half of aircraft structural failures are caused by fatigue which includes the oscillatory stress cycles that predominantly occur at the natural frequencies of the system [4]. Vibrations excited by diverse energy sources, such as external flows or internal vibrating machinery or motors, play a large part in the progressive fatiguing of structural panels such as those found on aircraft and have been intently studied in the past in order to understand the magnitude of their impact [5].

1.1 Review of previous research

To prevent the damage that results from systems encountering their resonances during operation, research efforts have focused on methods of vibration control that prevent systems from responding with the increased energy found at resonance. Research on effective structural vibration control methods has flourished, primarily on archetypal structures such as cantilever beams [6] [7] [8] [9] [10] [11] [12] [13]. Fully active feedback-based controls can provide useful vibration suppression for a wide range of working conditions [14] and with fast response time [15]. Additionally, piezoelectric materials can be embedded within or directly mounted on laminated structures such as those used in aerospace structures [9] [16] [17].

Yet, the added complexity of the electronic implementations, energy required to put the methods to practice, and the potential for loss-of-control are reasons to instead prefer *passive* or *passive adaptive* methods that address vibration concerns without such drawbacks. For example, recent studies have explored the viability of embedding temperature-sensitive silicone fluids within a straight channel inside of a cantilever beam where the modal frequencies of oscillation are seen to change due to the added fluid mass and its operating temperature [10]. Similarly, others have focused on the incorporation of nanoscale channels and fluids to tailor the damping properties and sensitivities of nanomechanical resonators [18]. Other studies have shown

that straight, fluidic passage networks attached to the top of a cantilever beam can change the natural frequencies of vibration due to characteristics similar to add-on vibration absorbers [11]. In addition, novel passive-adaptive vibration control can be achieved by using dynamic mass change on a cantilever beam due to free-sliding washers [12], while continued development of this idea has shown that a passive restoring force to return the free-sliding mass to a starting position enhances the vibration reduction [13]. Instead of attaching a vibration absorber to the structure, the change in eigenfrequency accomplished by strategies such as these allows the protected system to respond normally under excitation, rather than to resonate. Therefore, instead of transferring the resonant energy elsewhere in the system, these strategies remove the potential for resonant vibration in the first place.

1.2 New contributions from this research

While tuning vibration modes of nearly one dimensional structures such as cantilever beams has been explored via the static or dynamic addition or substitution of mass, the idea of designing mass distributions and internal channels for practical three dimensional structural systems has not been considered. This research explores the ability to tune low order vibration modes of structural panels with the transfer of mass in the form of fluid between strategically placed and designed voids via channels that connect them. The broader focus on three-dimensional structural panels opens up greater design flexibility for void shape, size, number, and location that may more dramatically and strategically tailor the vibration properties of structural systems commonly found in diverse engineering applications.

1.3 Research goal

The goal of this research is to use computational models and experimental validation to determine methods most useful to design "microvascular channels and voids" for structural panels to tune vibration properties in the most influential ways. Specifically, this research seeks to tailor the lowest order vibration modes of a structural panel because those are known to yield oscillations highest in amplitude. Considering the research motivation, achieving this goal may result in a new approach to maximize performance, integrity, and safety of structural panels as deployed in numerous engineering contexts via a straightforward passive-adaptive vibration control concept.

1.4 Overview of thesis

This thesis is organized as follows. Chapter 2 discusses the finite element model investigations conducted in this research and discusses methods of achieving structural panel dynamic performance with the inclusion of microvascular voids. Chapter 3 outlines the experimental processes undergone in order to validate the finite element model including specimen fabrication, 3-point bend tests, impact hammer experiments, and random excitation experiments. Finally, Chapter 4 summarizes the findings of the both the finite element model and the experimental results.

2 FINITE ELEMENT MODEL INVESTIGATIONS

2.1 Description of structural panel FE model

In previous research performed on the vibration control of structures, the use of finite element modeling has been employed as a first stage and primary effort to investigate the effect of these vibration control methods on the system of interest. Due to its ability to permit the user to design the model, make adjustments, and perform iterative investigations, finite element modeling is useful for investigating and gaining insight on a problem before and after making a proof of concept prototype [1] [2] [7].Similarly, for this research, COMSOL Multiphysics finite element modeling (FEM) software is used to model the structural panel. The structural panel FE model without voids is 12.7 cm x 8.46 cm x .32 cm, according to the experimental system studied in the other efforts of this research. The panel in the FE model includes either fixed-free or free-free boundary conditions where the 8.47 cm side is the fixed end in the fixed-free scenario. The material properties are for acrylic plastic and include:

$$\rho = 1190\frac{kg}{m^3},\ E = 2E9Pa,\ \nu = .35$$

Preliminary results show that the fixed-free panel has first, second, and third eigenfrequencies of approximately 275 Hz, 375 Hz, and 756 Hz while the free-free panel has first, second, and third eigenfrequencies of 285 Hz, 324 Hz, and 689 Hz. The corresponding von Mises stress variations and mode shapes for the fixed-free and free-free panel, respectively, are shown in Figure 1 and Figure 2. It is important to note that for the free-free boundary condition panel, the accelerometer is incorporated into the FE model to account for its mass loading effects, as seen in Figure 2.

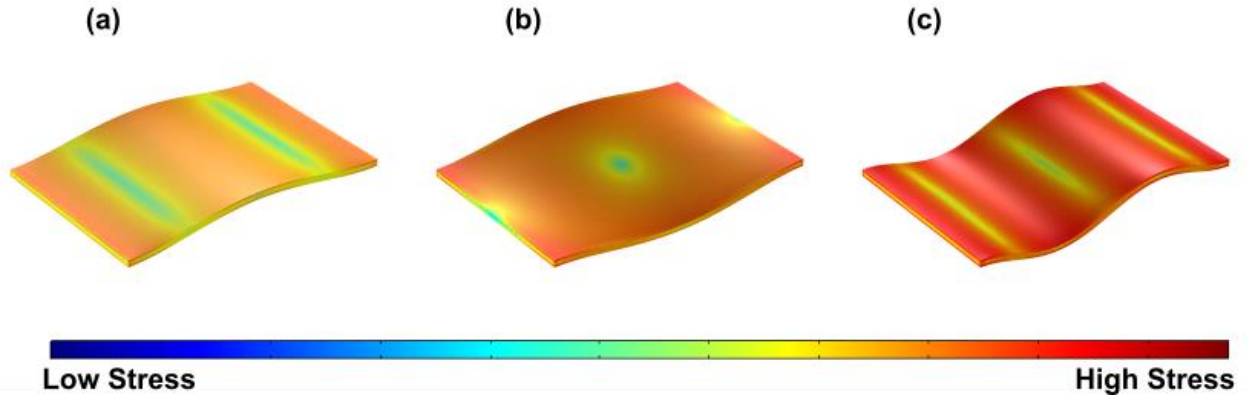

Figure 1. Von Mises stress distributions of the (a) first, (b) second, and (c) third mode shapes of the fixed-freeFE model

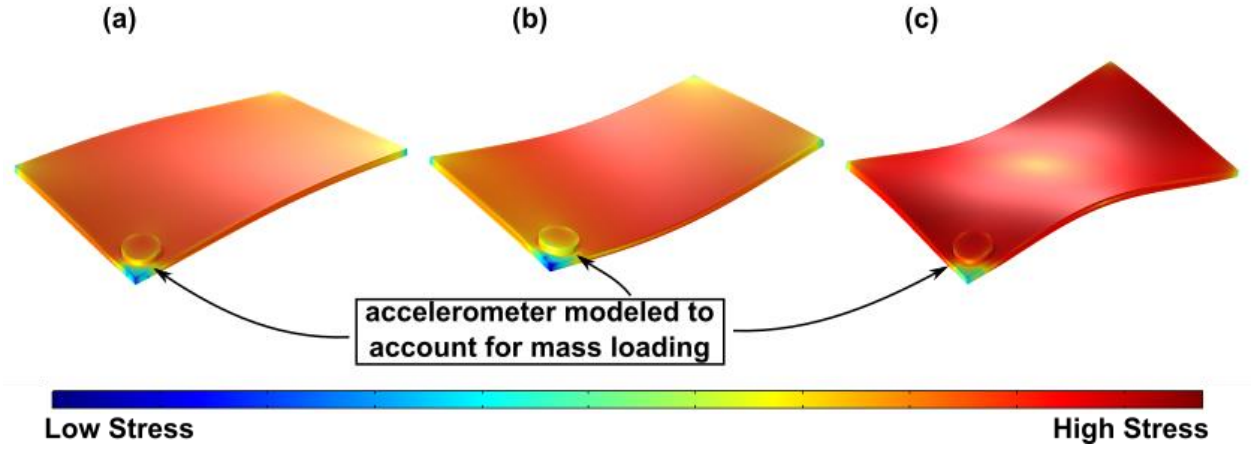

Figure 2. Von Mises stress distributions of the (a) first, (b) second, and (c) third mode shapes of the free-free FE model

The FE model is used to replicate a scenario in which fluid is transferred into and out of voids embedded within the structural panel in an effort to tailor the dynamic performance of the panel as seen in Figure 3. The voids, when incorporated, constitute removal of the middle 1/3 of panel thickness, as seen in Figure 4.

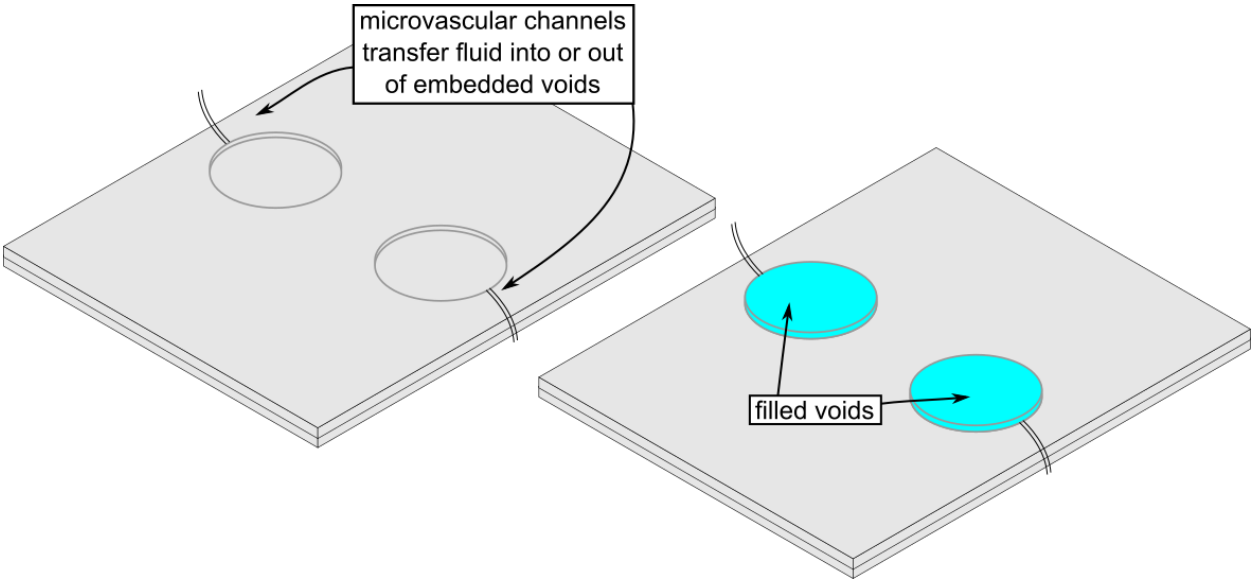

Figure 3. The FE model is used to replicate a scenario in which fluid is transferred into or out of voids embedded within the structural panel via microvascular channels

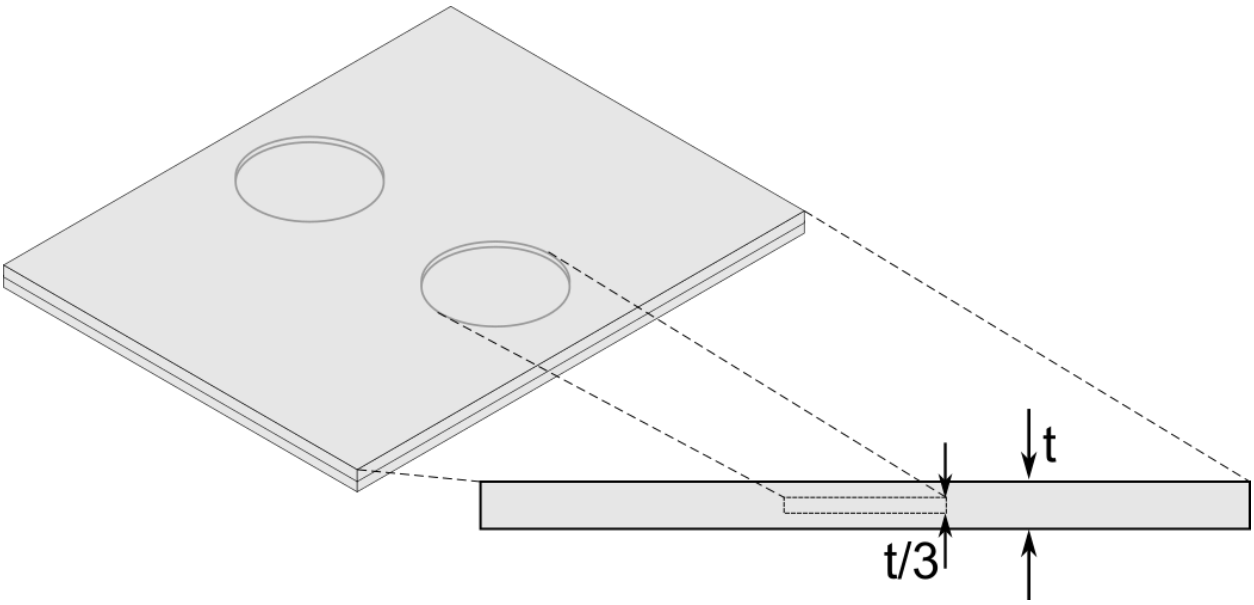

Figure 4. The voids, when incorporated in the panel, constitute removal of material in the middle third of the panel thickness

2.2 Finite element model assumptions and analysis conventions

For a first approximation of the roles of fluid-filled voids, in the FE models it is assumed that the density of the fluids filling the voids in the panels is the same as that of the panel and that the fluid is a solid. In this way, a completely filled void can be modeled as an unvoided panel, as seen in Figure 5. Furthermore, the contributions to the mechanical and dynamic behavior made by the microvascular channels that connect the voids are assumed to be negligible and are thus omitted from the FE model to reduce complexity and computation time. Additionally, in FE model computations and analyses presented hereafter, the percent change in eigenfrequency is calculated as a difference between the eigenfrequencies of a panel with completely filled and completely empty voids.

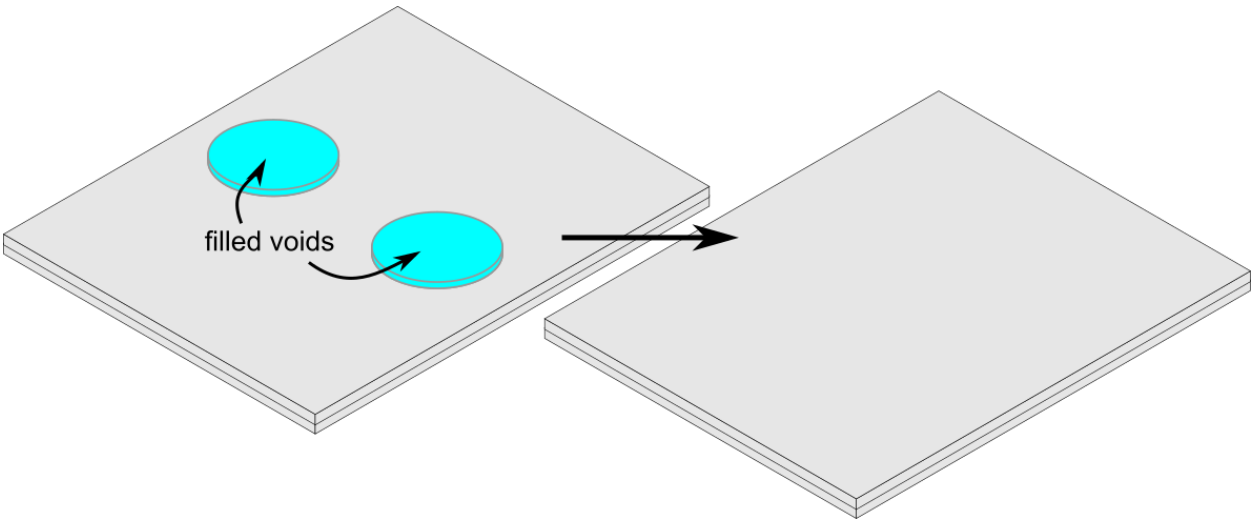

Figure 5. A panel with filled voids is modeled as an unvoided panel in order to simplify the FE model

2.3 Investigation of influence of void shape on panel eigenfrequencies

Previous research has shown that a movable mass on a cantilever beam is one method to realize tunable vibration control [12] [13]. Having a variable stiffness is another way of controlling the natural frequencies of a system [19]. These concepts in which the mass and stiffness of the structures are altered to accomplish tunable vibration control set the precedent for the following studies in which voids, that can be filled or empty, are varied across the panel in areas of differing stress and displacement. The voids act as a tunable change in system mass and stiffness characteristics. Going beyond previous research that has focused on one-dimensional cantilever beams, the influence of how three-dimensional void characteristics come into play when considering the advantages that can be leveraged with respect to void shape, number, size, and location is studied in the following investigations. In the first study, a set of two circular and square voids of equivalent mass removal are placed in and varied across the structural panel as seen in Figure 6.

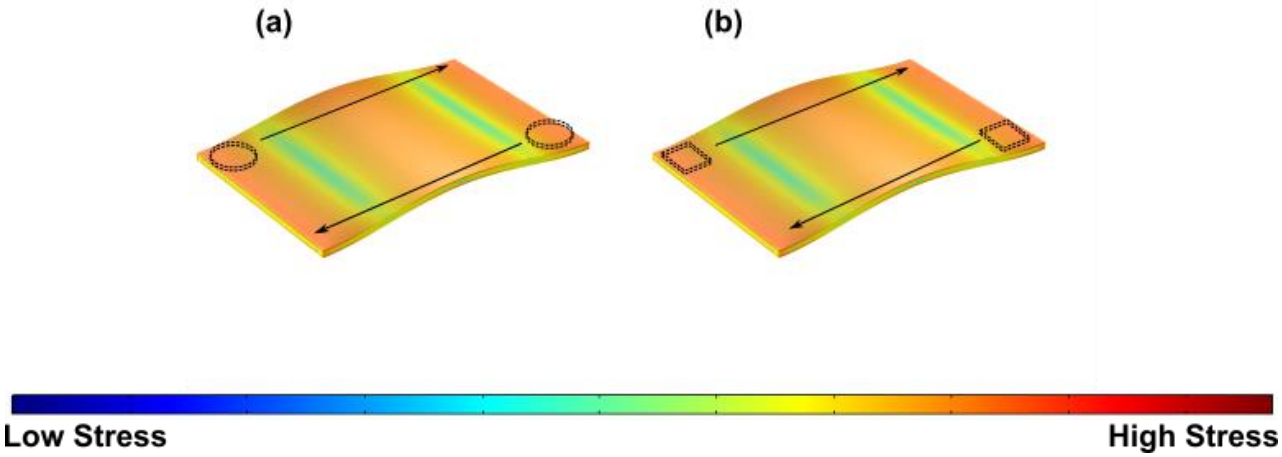

Figure 6. Shown on the first mode stress distribution of the panel, (a) circular and (b) square voids are varied across regions of high and low stress and displacement in order to reveal the influence of void shape on change in eigenfrequency

The one-dimensional nature of cantilever beams limits the importance of investigating different shapes of mass removal; however, the influence of void shape on the dynamic performance of three dimensional structures is unknown. Thus, a removal of mass in the form of voids of different shape at locations of varying degrees of stress is used as a first effort to change the eigenfrequencies of the panel and investigate the role that void shape plays in this change. The location of a pair of either circular or square voids is varied across the panel to reveal the influence of void shape on change in eigenfrequency. As seen in Figure 7 where the percent change in eigenfrequency as a result of void inclusion is shown according to where the voids are placed in the panel, with equivalent mass removal, circular and square voids share nearly identical eigenfrequency changing characteristics. In addition, although different void shapes influence the eigenfrequencies of the panel nearly identically, a difference in eigenfrequency change can be seen with respect to where the voids are placed, which is investigated in a following study. Due to the desire to avoid stress concentrations and the lack of evidence to point to a void shape-dependent nature of the eigenfrequencies of the panel, circular voids are chosen for subsequent investigations.

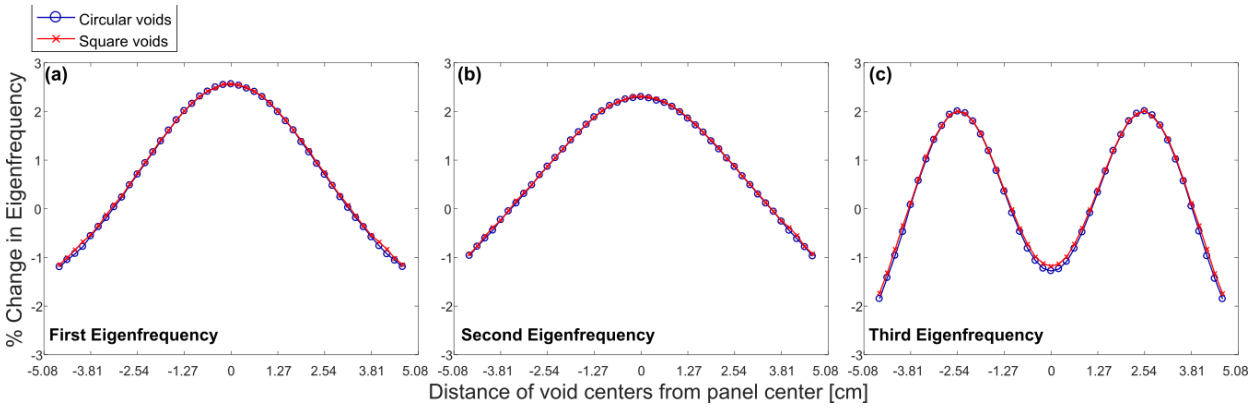

Figure 7. Percent change in eigenfrequency due to circular and square voids for the (a) first, (b) second, and (c) third eigenfrequencies of the structural panel

2.4 Investigation of influence of void number and size on panel eigenfrequencies

Research on the use of tuned mass dampers within buildings shows that, in such structures, the use of multiple tuned mass dampers is ideal in preventing modal responses under excitations caused by earthquakes [20]. From this, as the addition or removal of mass in the form of voids serves as a form of vibration adjustment device for the panel, the use of multiple voids in the panel is investigated. Additionally, as the mass characteristics of the system are important in determining its frequency response, the influence of the size of the voids on their ability to change the eigenfrequencies of the system is also investigated. Similar to the FE model used to study the influence of void shape on the percent change in eigenfrequency, the void(s) is/are varied across the panel, as seen in Figure 8.

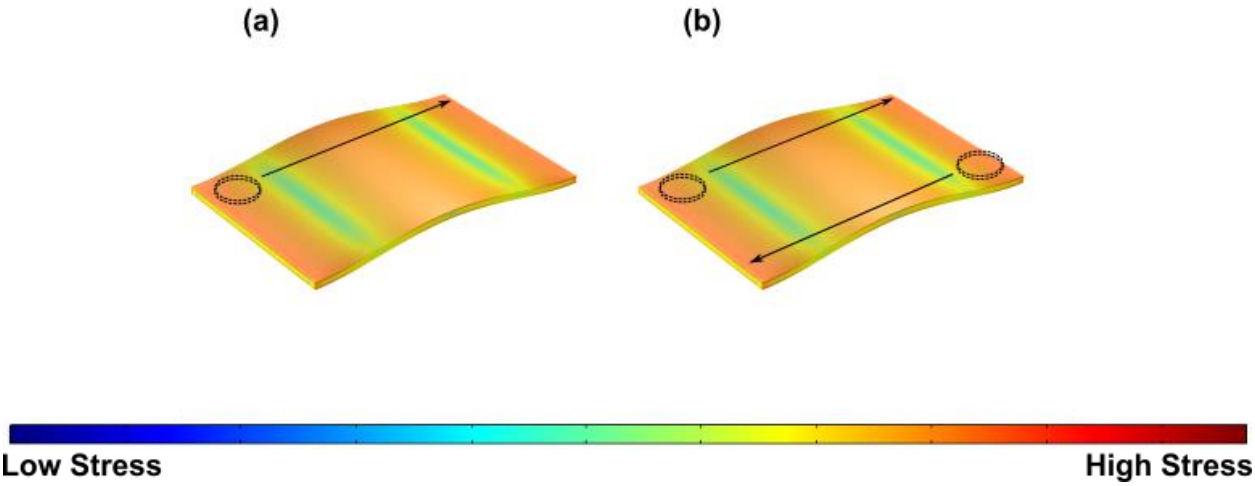

Figure 8. Shown on the first mode stress distribution of the panel, the role of (a) one versus (b) two voids is investigated for its ability to change the eigenfrequency of the FE model

As seen in Figure 9 where the change in eigenfrequency is shown according to void location, the scenario in which two voids are used is always more influential compared to the single void case in terms of magnitude of percent eigenfrequency change, except for the case in which the change is zero. This trend may be due to a relationship between the amount of mass removed and the net influence on change in the eigenfrequencies of the system, in contrast to the mass removal undertaken using multiple voids. The point of zero eigenfrequency change, which occurs for both the single and double void cases at the same location in the panel, indicates that there exists a solely location dependent ability of the voids to influence the eigenfrequencies of the panel. At void locations around this point, the voids have an either positive or negative influence on the percent change of the eigenfrequencies of the panel.

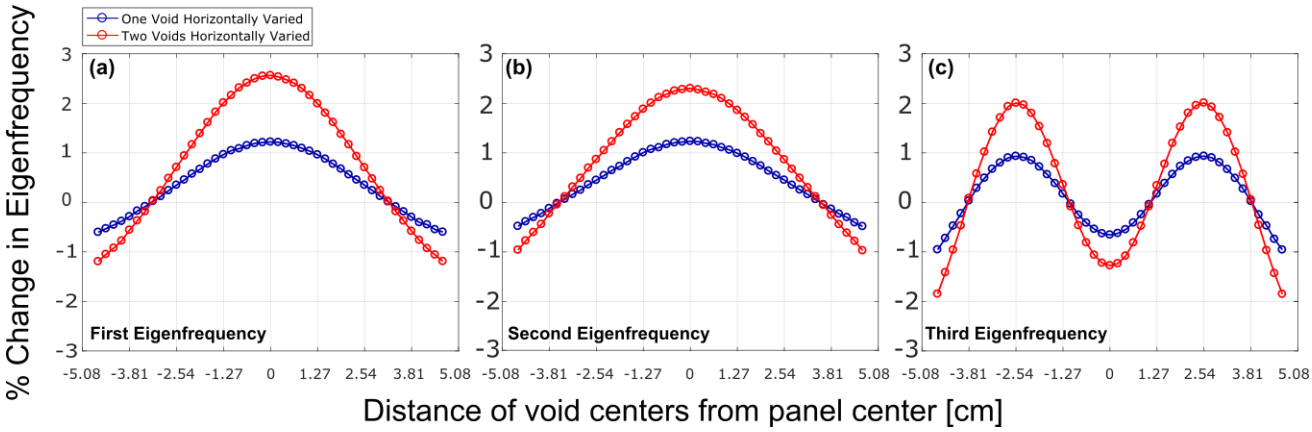

Figure 9. Percent change in (a) first, (b) second, and (c) third eigenfrequencies according to void number and their location

Next, in order to investigate the influence of void size on the percent change in eigenfrequency, two sets of void locations with changing radii are placed on regions of differing stress and displacement, as seen in Figure 10. These two void sets are termed corner voids and center voids for the sake of this comparison.

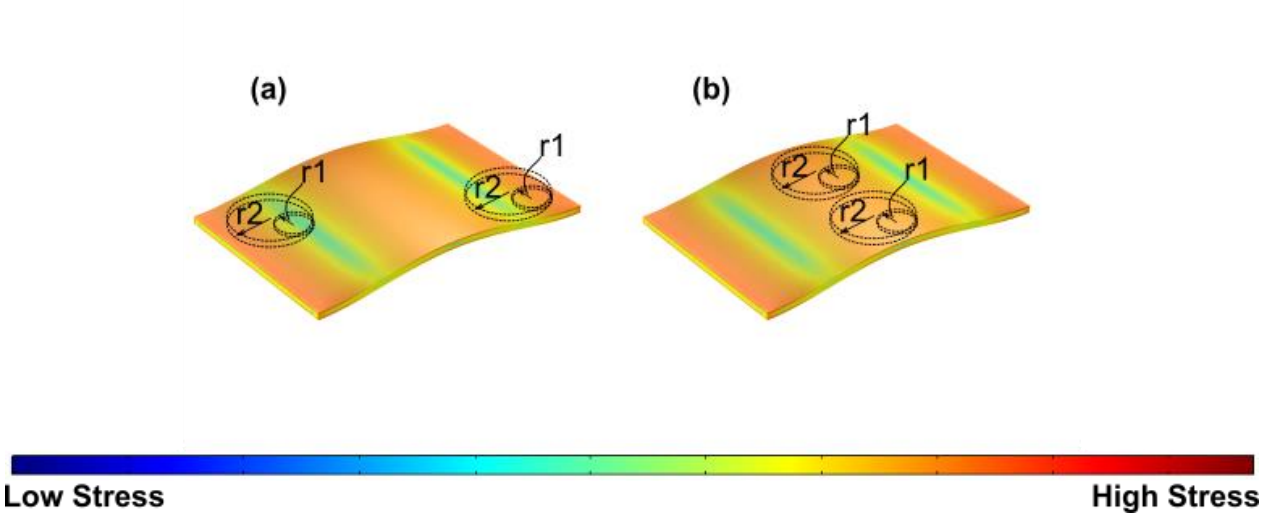

Figure 10. Shown on the first mode stress distribution of the panel, two sets of void locations are used in order to investigate the role of void size on its ability to change the eigenfrequencies of the panel: (a) corner voids and (b) center voids

As seen in Figure 11 where the change in eigenfrequency is shown according to the radius of the voids, larger sized voids correspond to larger eigenfrequency changes, in general. Additionally, it can be noted that each eigenfrequency is affected differently in terms of the amount of influence that the void size has on its change in value. This dependence on location is explored in greater detail in the following study.

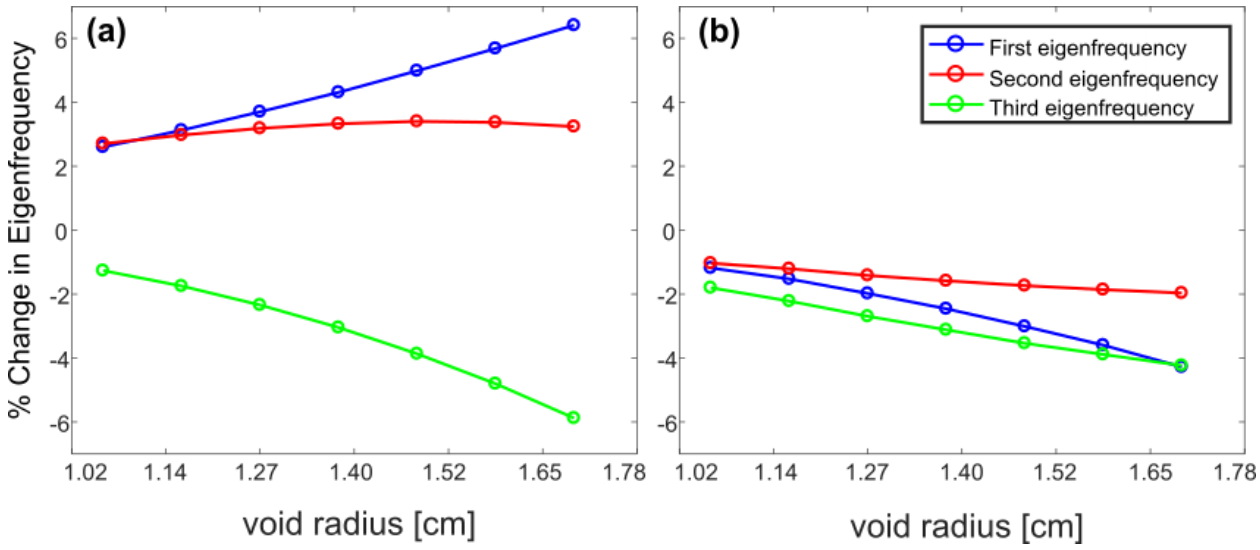

Figure 11. Percent change in eigenfrequency as a function of void size for (a) corner and (b) center voids, as termed above

2.5 Investigation of influence of void location on panel eigenfrequencies

From sections 2.3 and 2.4, a greater percent change in the first three eigenfrequencies of the structural panel corresponds to voids higher in number and larger in size, or, equivalently, of larger mass removal. Considerations of the relationship between eigenfrequency change and placement of voids with respect to

panel mode displacement are taken into account for the following study. A total of two voids per study are used; two termed horizontal voids and two vertical voids, so called because of the way in which they are varied across the panel, as seen in Figure 12.

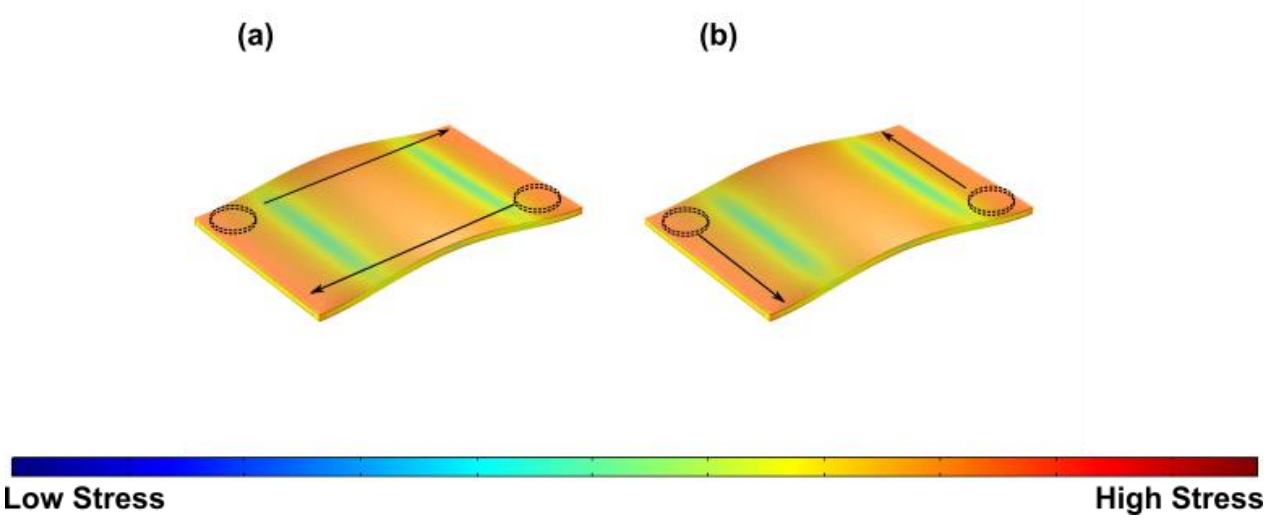

Figure 12. Shown on the first mode stress distribution of the panel, two sets of voids are varied (a) horizontally and (b) vertically

Figure 13 shows that the percent eigenfrequency change differs in both magnitude and sign for different void locations in the panel. For better visualization, Figure 14 shows that, for a percent change in eigenfrequency evaluated based on fluid flow out of voids according to their placement within the panel, positive and negative eigenfrequency change corresponds to void placement in areas of higher and lower displacement, respectively. This is hypothesized to be due to the possibility that areas of highest amplitude displacement are dominated by inertial effects due to their larger displacements and are thus highly influenced by mass removal in a way that increases eigenfrequency. Conversely, areas of lower displacement magnitude near the clamped edges, or alternatively areas of higher stress, are influenced by mass removal in a way that decreases eigenfrequency.

Considering the equation for the natural frequency of a single degree-of-freedom dynamic system, $\omega_n = \sqrt{\frac{k}{m}}$ where k is the stiffness and m the mass of the system, in the portions of the panel of highest modal displacement, mass removal has less of an influence on the stiffness of the panel and corresponds to an increase in eigenfrequency. Alternatively, in the stiffness dominated portions of the panel with lower modal displacement and higher stress, mass removal corresponds to a large decrease in stiffness, or equivalently, a decrease in eigenfrequency.

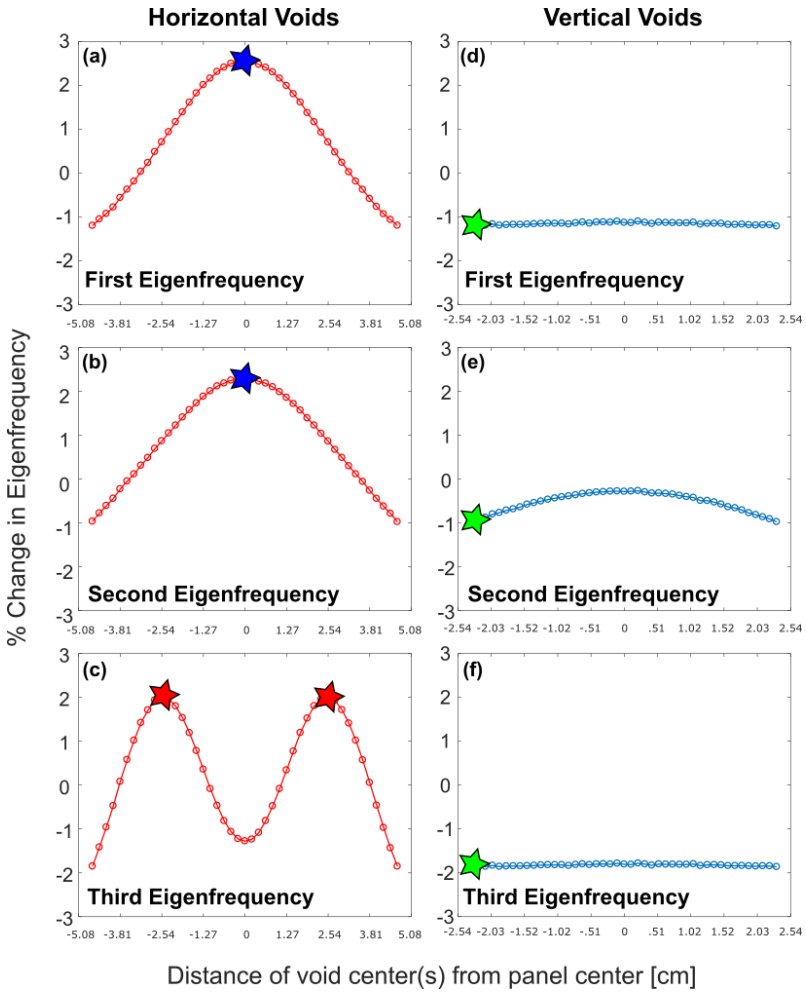

Figure 13. Percent change in eigenfrequency for horizontal and vertical void placement, as defined above. Stars represent chosen void location, as detailed and later referenced in Figure 17

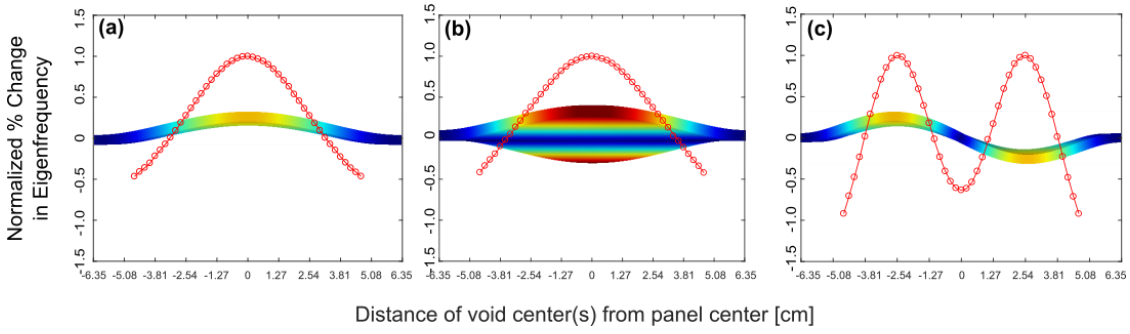

Figure 14. Percent change in (a) first, (b) second, and (c) third eigenfrequency according to void location. Plots overlaid on front views of modal displacements to emphasize relationship between eigenfrequency change and placement of voids with respect to modal displacement

2.6 Results and discussion

Summarizing the efforts of this chapter, the void shape, size, number, and location are investigated in the FE model with respect to how much they are able to change the eigenfrequencies of the structural panel First, it is found that void shape has little effect on the eigenfrequency change of the panel. It is instead found that increasing magnitude of eigenfrequency change is related to voids larger in size and higher in number. Such a trend may be anticipated to be solely due to the quantity of mass that is removed. Void location also appears to be influential in changing the eigenfrequencies of the panel. Void placement, and therefore mass removal, in areas of higher displacement results in increases in eigenfrequencies while an equivalent mass removal in areas of higher stress results in decreases in eigenfrequency.

Considering the equation for the natural frequency of a single degree-of-freedom dynamic system, $\omega_n = \sqrt{\frac{k}{m}}$, it can be seen that in regions of higher displacement and stress, the mass and stiffness, respectively, must have more influence on the change in eigenfrequencies of the system. In order to maximize the achievable percent change in eigenfrequency, a fluid transition between voids in each of these locations can be utilized such that, with respect to the eigenfrequencies of the unvoided panel, the change occurs between a maximum (in magnitude) positive change in eigenfrequency and a maximum (in magnitude) negative change in eigenfrequency.

From the plots in Figure 13, void locations can be chosen in order to achieve this change. Furthermore, as seen in Figure 14, the achievable increases in eigenfrequency by void inclusion are more impactful than the achievable decreases in eigenfrequency. This may be a result of mass removal in areas of higher stiffness constituting a large reduction in both stiffness and mass where these have opposite influences in terms of trend of eigenfrequency change. On the other hand, mass removal in areas of higher displacement, where inertial effects are assumed to be more influential than stress and stiffness effects, provides a greater magnitude of eigenfrequency change. According to the FE model, placing two sets of two voids of radius 1.69 cm in the strategic locations mentioned in section 2.5 will allow for a maximum percent eigenfrequency change of 10.0%, 5.0%, and 7.4% for the first, second, and third eigenfrequencies, respectively, according to a fluid transition between void sets. This can be seen in Figure 15 where the percent changes in eigenfrequency are shown according to void size. The void sets would comprise of one horizontal and one vertical void set, as termed previously, and could be used to most strategically target the first and second eigenfrequency simultaneously or the third by itself. These panel configurations will serve as the designs used for experimental validation.

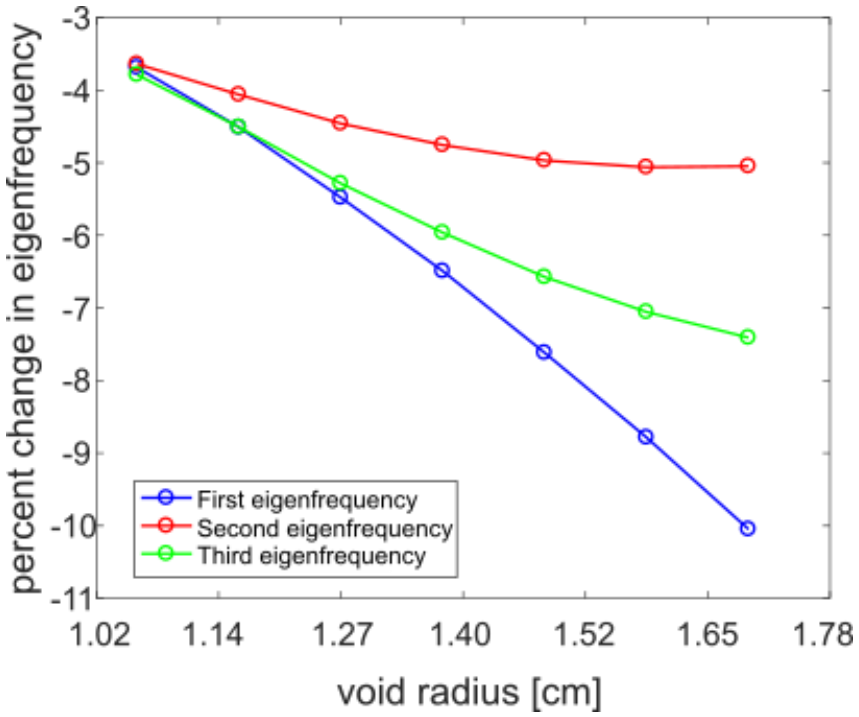

Figure 15. Percent eigenfrequency change achievable with void sets as prescribed, shown according to growing void radius

3 EXPERIMENTAL VALIDATION

Three sets of experiments, 3-point bend, impact hammer, and random excitation, are performed in order to update the material properties of the FE model as well as for experimental validation of the key FE model predictions described in Chapter 2. Two sets of proof of concept specimens are fabricated because the impact hammer and random excitation experiments share the same specimens. The specimens are tested for their density and stiffness properties and structural integrity after fabrication in the 3-point bend tests. Impact hammer and random excitation tests are performed in order to validate the predictions made by the FE model.

3.1 Fabrication of 3-point bend, impact hammer, and random excitation test specimens

3.1.1 Fabrication methods

Transparent, .16 cm acrylic sheets (McMaster-Carr, 8560K171) are used for the halves of each experimental specimen for 3-point bend, impact hammer, and random excitation tests. A laser cutter (Full Spectrum LASER H-Series 20x12 Desktop CO2 Laser) is used to both engrave voids within the acrylic as well as to cut specimens out of the acrylic sheets. For all specimens, acrylic cement (TAP Acrylic) is applied to the inner faces of the panels which are then set to cure for at least 48 hours. These fabrication steps are illustrated in Figure 16.

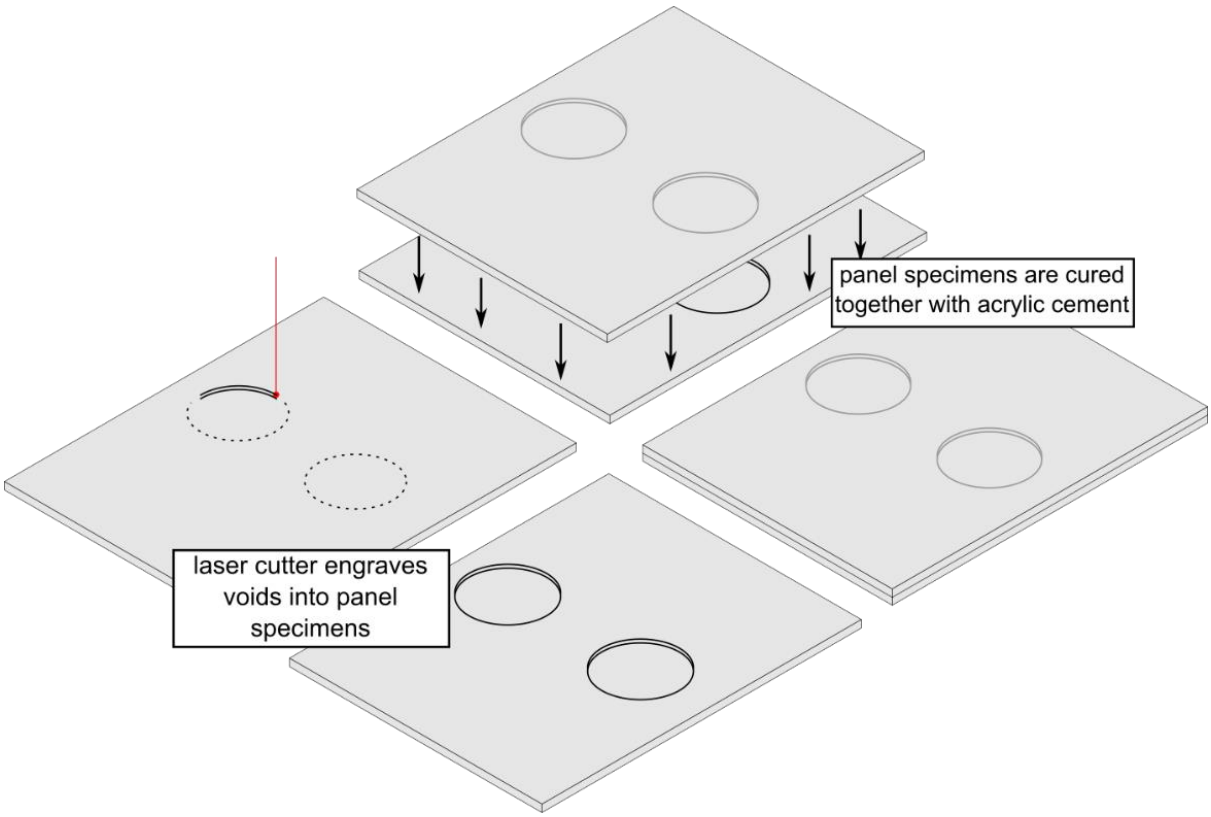

Figure 16. Specimen fabrication. Voids are first engraved into acrylic sheets before the two sheets are cured together

3.1.2 Fabricated specimen dimensions

For the 3-point bend tests, two halves of each specimen are cut out of the acrylic to be 10.16 cm x 6.35 cm in their length and width dimensions and combined to form the final three specimens of .32 cm thickness. For the impact hammer and random excitation experiment specimens, half of each void is engraved into each half of the specimen so that when combined, the voids would be centered with respect to the thickness of the panel. Four panel specimens are fabricated for these tests: an unvoided panel (specimen N-V), a panel with voids near the first, second, and third displacement nodes (specimen 1-2-3-N), a panel with voids on the first and second eigenfrequency displacement antinodes (specimen 1-2-A), and a panel with voids on the third eigenfrequency displacement antinodes (specimen 3-A). For specimen 1-2-3-N, this corresponds to voids centered at [2.36 cm, 2.36 cm] and [10.34 cm, 6.10 cm] with respect to a 12.70 cm x 8.46 cm panel whose origin is one of its corners. The actual panel is fabricated to be 12.70 cm and .95 cm on its longest dimension to allow for clamping; however, the voids are still placed as if the extra .48 cm on each side is neglected. Specimen 1-2-A has voids at [6.35 cm, 2.36 cm] and [6.35 cm, 6.10 cm] while the voids for specimen 3-A voids are placed at [3.81 cm, 6.10 cm] and [8.89 cm, 2.36 cm]. These void locations are outlined below in Table 1, the voids plotted with respect to a top down view of the displacement distribution of the panel are shown in Figure 17, and the fabricated specimens are shown in Figure 18.

Table 1. Specimen IDs and the corresponding locations of their voids

Specimen ID	Void Coordinate 1, X,Y [cm]	Void 2 Coordinate 2, X,Y [cm]
N-V	N/A	N/A
1-2-3-N	2.36, 2.36	10.34, 6.10
1-2-A	6.35, 2.36	6.35, 6.10
3-A	3.81, 6.10	8.89, 2.36

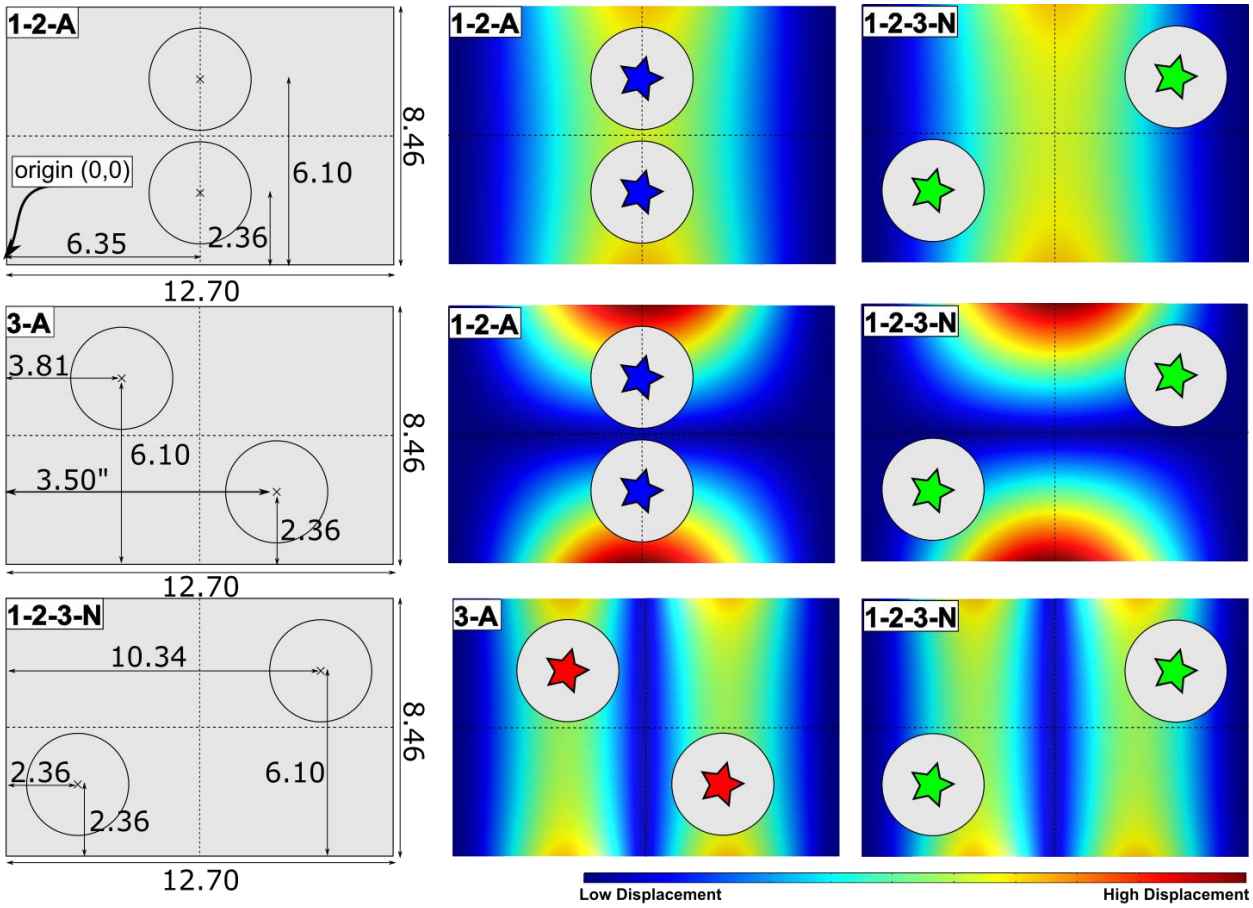

Figure 17. Fabrication plan for panel specimens with voids. Starred voids reference locations that are determined to be ideal for strategic void location, as seen in Figure 13. Dimensioned in [cm]

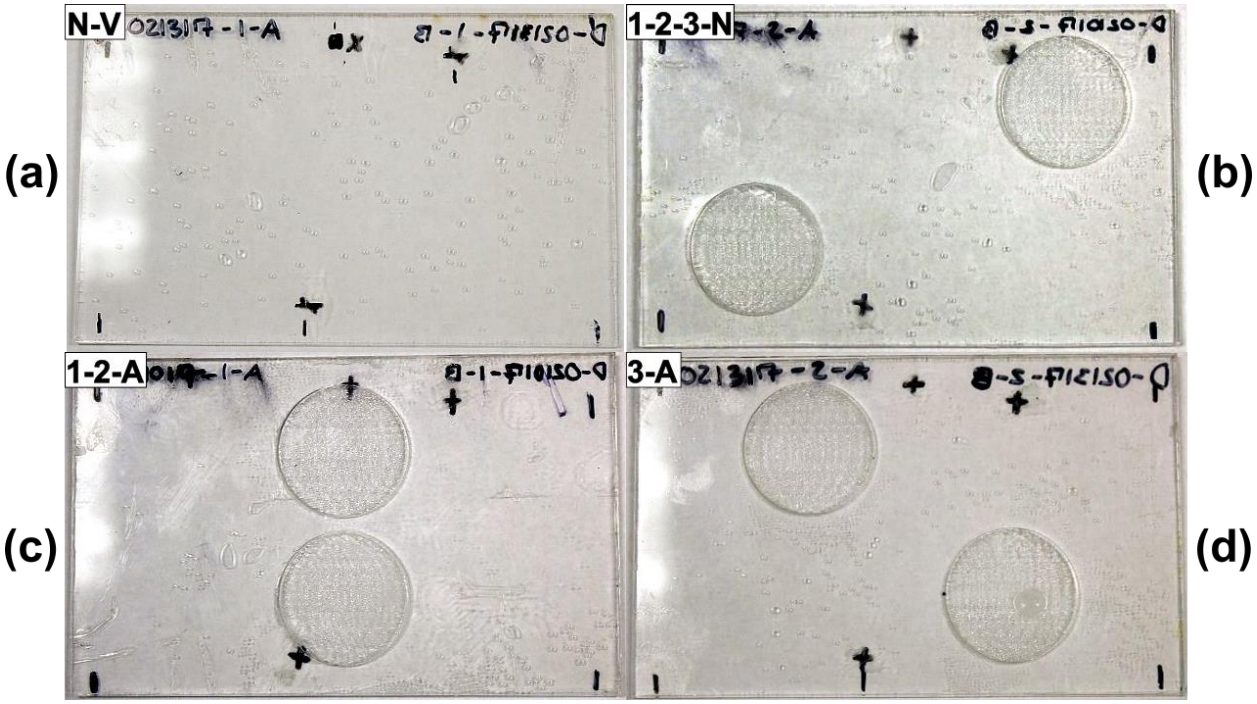

Figure 18. Fabricated specimens: (a) N-V, (b) 1-2-3-N, (c) 1-2-A, and (d) 3-A

3.2 Three-point bend tests

3.2.1 Sensors, equipment, and data acquisition methods

Specimens are fabricated for 3-point bend tests in order to characterize specimen density as well as the stiffness of the cured panels, as seen in Figure 19. Additionally, as curing bubbles of varying degree appear after the specimens have cured, the 3-point bend tests help evaluate the degree to which the bubbles may influence the stiffness of the specimens. The tests are conducted on an isolation table (Newport SMART TABLE UT2). A linear hand cranked load frame (Mark-10 ES20) with a displacement of 2.1 mm per revolution is used to move the load cell (PCB 1102-05A) up and down at a rate of one hand crank per minute to result in a displacement loading rate of 2.1 mm per minute. The displacement of the load cell is monitored by a laser displacement sensor (Micro Epsilon ILD-1700-200). The specimens are placed on top of two cylindrical, aluminum mounts that are rigidly attached to the isolation table. A third aluminum cylinder is mounted to the load cell for specimen loading. Before each test, the top cylinder is set to load the specimen to help ensure uniform and centered contact during the test that follows. Data is sampled at 256 Hz with a low pass cutoff frequency of 35 Hz for 130 seconds to account for a minute of increasing displacement, a minute of decreasing displacement, with 10 seconds to ensure all of the data is captured. An example MATLAB code used for data acquisition and post processing is shown in the appendix.

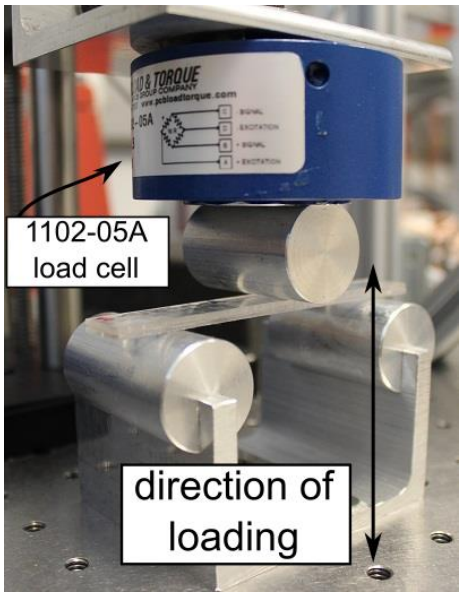

Figure 19. Experimental setup of 3-point bend test to characterize specimen stiffness and evaluate the effect of curing bubbles within specimens

3.2.2 Results and discussion

Three specimens are fabricated according to the methods outline in section 3.1 in order to characterize the stiffness of the cured specimens and evaluate the effect of curing bubbles. The specimens each undergo a 3-point bend test that reveals that each have a very similar stiffness, as seen in the slopes of the load-displacement data in Figure 20.

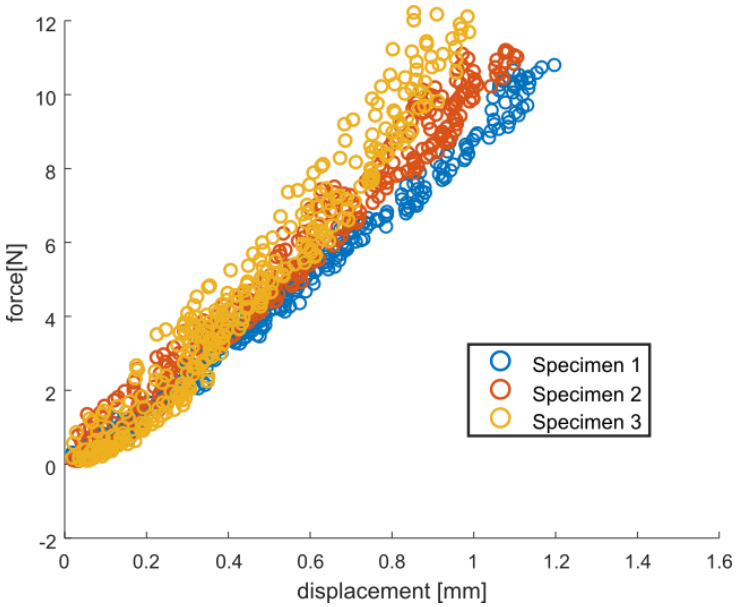

Figure 20. Force- displacement plot for the 3-Point bend test specimens

The specimens are then used to calculate the density of the acrylic as $\rho = Lwt$ where L = length of the specimen, w = width, and t = thickness. Next, the Young's Modulus of the acrylic is calculated from classical beam theory according to $E = \frac{PL^3}{48 w_0 I}$ where P = applied force, L = length of specimen, w_0 = beam deflection, and I = second moment of area = $\frac{t^3 w}{12}$. Table 2, below, displays the results of these calculations which are then used to modify the FE model to increase its accuracy specifically for the fabricated specimens which have properties slightly different than those of the model due to the fabrication methods.

Table 2. Adjusted FE model parameters according to experimental results

Corrected Parameter	Value
Density [kg/m^3]	1112
Young's Modulus [Pa]	3.8E9

After curing, each specimen exhibits a certain degree of curing bubbles. These bubbles are colored in Adobe Photoshop and are characterized by the surface area they cover as a percentage of the surface area of the top of the specimen they are found in, as seen in Figure 21. The percentage of specimen surface area occupied by curing bubbles is then compared against recorded stiffness values for each 3-point bend test specimen to see if the bubbles had a significant impact on the stiffness of the specimens, as seen in Table 3.

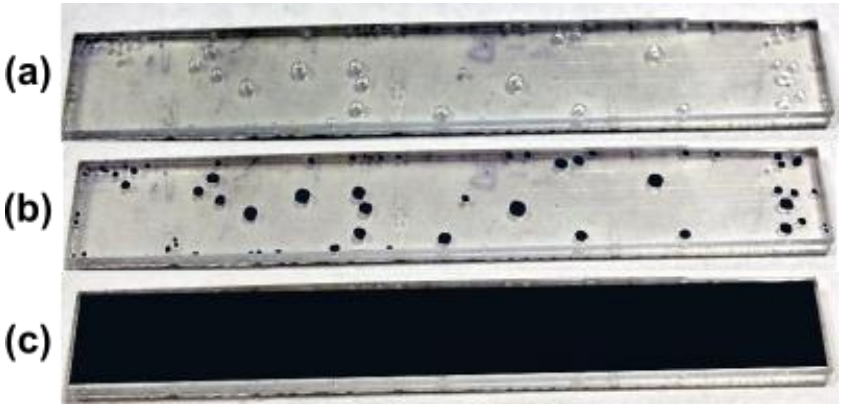

Figure 21. (a) Image of specimen with curing bubbles, (b) image of specimen with curing bubbles colored, and (c) image of specimen with top surface area colored. The ratio of the colored portions of (b) and (c) serves as an evaluation of how many curing bubbles are in a specimen

Table 3. Percentage of surface area occupied by curing bubbles and measured stiffness for 3-point bend specimens

Specimen #	Percentage of surface area occupied by curing bubbles	Measured Bending Stiffness [kN/mm]
Specimen 1	0.49%	10.97
Specimen 2	5.22%	10.86
Specimen 3	5.42%	11.41

Table 3 shows that, to the extent measured, the bubbles do not seem to have a significant impact on the stiffness of the specimens. Specifically, whether having about 0.49% or as much as 5.42% bubbles within the specimens after the curing process, the bending stiffness deviates only by about 4.0%. Thus, the amount of curing bubbles that are developed in consequence to the current fabrication process is not anticipated to significantly influence the results of the following investigations of the panel dynamics.

3.3 Impact hammer experiments

3.3.1 Sensors, equipment, and data acquisition methods

Impact hammer experiments are performed on free-free boundary condition panel specimens as a first step in validating the predictions made by the FE model. The specimens, suspended by fishing line as seen in Figure 22, are struck by an impact hammer (PCB 086C02) in nine different locations and their acceleration is measured with a mini-accelerometer (PCB U352B22). These signals are then processed in a data acquisition unit (LMS SCADAS Mobile SCM01). Using LMS Test Lab 16A Impact Testing software, the measured mode shapes of each panel specimen are correlated to the mode shapes predicted by the FE model. The resulting eigenfrequencies both measured in experiment and predicted by the FE model are compared to validate the accuracy of the FE model.

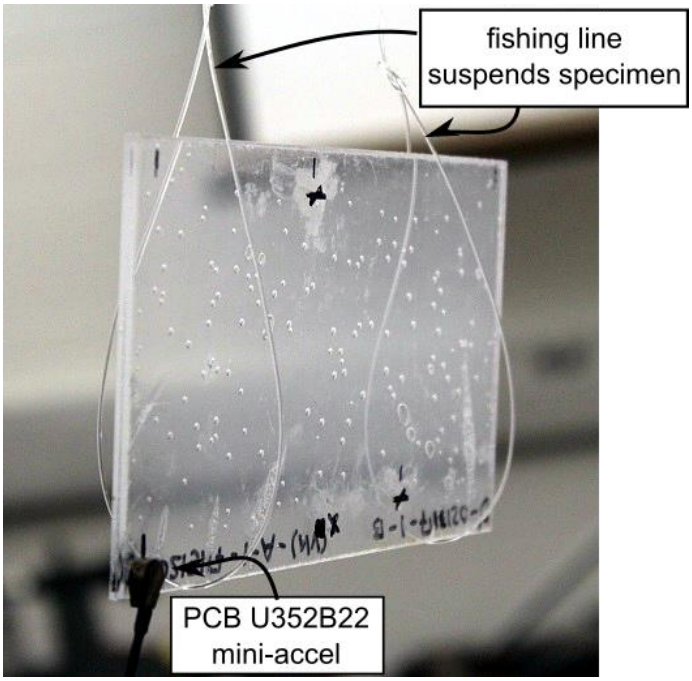

Figure 22. Free-free boundary condition experiments are performed on the specimens to validate FE model predictions

3.3.2 Results and discussion

Finite element model and experimental mode shapes for specimen N-V are shown below in Figure 23. The LMS software is able to accurately measure the mode shapes of the panel which corresponded to those predicted by the FE model. The eigenfrequencies of the experimental and FE model results then are used as a source of comparison to validate the results predicted by the FE model as seen in Table 4 according to the specimens as seen in Figure 18.

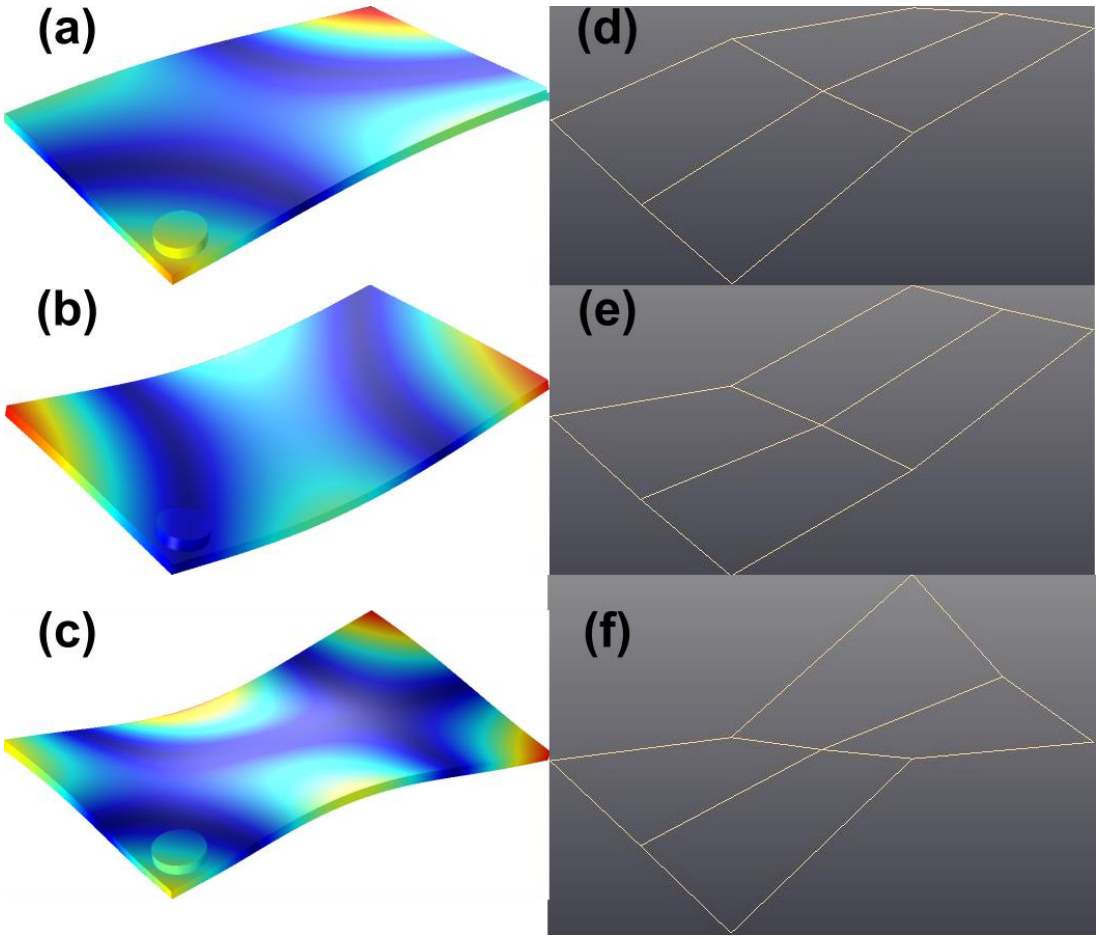

Figure 23. FE model predictions for the displacement distributions of the first three free-free panel eigenfrequencies for specimen N-V ((a), (b), and (c), respectively) are compared against LMS software mode shape results ((d), (e), and (f), respectively) in order to see the difference between FE model and experimental results

Table 4. Comparison of FE model predictions and experimental results for eigenfrequencies of the panel specimens under a free-free boundary condition

	First Eig. [Hz]		**Second Eig. [Hz]**		**Third Eig. [Hz]**	
Specimen ID	FE Model	Exp.	FE Model	Exp.	FE Model	Exp.
N-V	283	284	315	306	678	665
1-2-A	270	251	307	280	653	633
3-A	279	271	310	300	660	618
1-2-3-N	281	264	318	294	677	624

As can be seen in Table 4, predictions made for the unvoided specimen (N-V) remain within 13 Hz of experimental data while those made for the voided specimens deviate as much as 53 Hz. This is likely due

to the bonding layer being a source of stiffness and damping, incomplete bonding around void edges, or local softening of voided areas due tosolvent based acrylic cement. Yet, the experimental data exhibits the trends that the FE model predicts, serving as validation. It is important to note that large changes in panel eigenfrequencies in the free-free boundary condition panel are not predicted by the FE model or experiments. This is possibly due to the fact that the mode shapes and stiffness characteristics of the free-free boundary condition FE model are different than those of the fixed-free FE model. Thus, the voids that have been designed to most strongly influence the eigenfrequencies of the fixed-free panel are not applicable in terms of achieving high percent eigenfrequency change in the free-free boundary condition FE model.

3.4 Random excitation experiments

3.4.1 Sensors, equipment, and data acquisition methods

Random excitation experiments are performed on fixed-free boundary condition panel specimens in order to characterize the frequency response of the panel specimens for additional experimental validation of the FE model results. The experiments are performed on an isolation table (Newport SMART TABLE UT2). A shaker (LabWorks LT-140-110) is controlled by a controller (Vibration Research VR9500) whose outputs are sent to a power amplifier (LabWorks PA-141) that is connected to the shaker. Data is collected by MATLAB version R2016b which uses a script file and data acquisition (NI DAQ) toolbox to acquire and process data. An accelerometer (PCB 352C33) is placed on the shaker and serves as a measurement for the control acceleration while three accelerometers (PCB 352A24) are placed on the panel specimens to measure the output panel acceleration, as seen in Figure 24. For the random excitation experiments, the panel specimens undergo excitation between a range of 50 and 2000 Hz and are sampled at a frequency of 16384 Hz for a total experiment time of one minute. Three total experiments are conducted for each panel to ensure consistency in clamping for each specimen. The output acceleration of each accelerometer divided by the acceleration of the shaker, constituting the frequency response transfer function, is averaged in the individual experiments and are compared against each other to visualize the resulting eigenfrequency shifts between panel specimens.

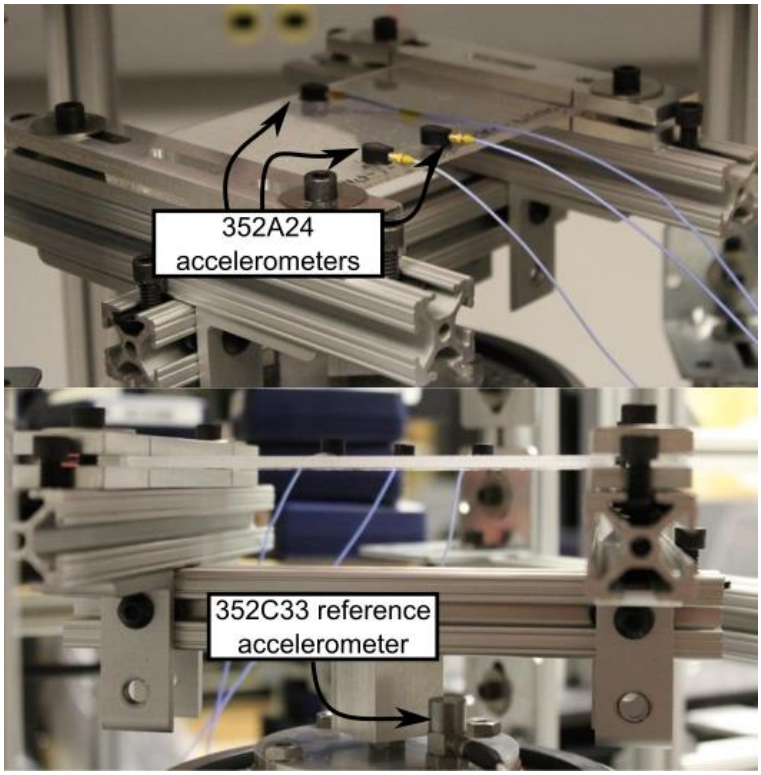

Figure 24. Experimental setup for random excitation experiments to evaluate frequency response of panel specimens

3.4.2 Results and discussion

Four panel specimens are fabricated according to the methods outlined in section 3.1. As stated previously, in order to account for the length of the panel lost to clamping, the specimens are fabricated with an extra 0.48 cm on each side of their longest dimension such that when clamped, the remaining panel area is 12.7 cm x 8.46 cm. The frequency response transfer function in dB is computed as the output acceleration, measured on the panel by the average of the aforementioned accelerometers, divided by the input acceleration, measured on the shaker. Three experiments that are undertaken to check for consistency in clamping between experiments are shown for specimen N-V in Figure 25. The results show that after re-clamping the specimen between experiments, the data remains consistent, which is important to show that the boundary condition can be replicated despite the fact that acrylic, which is soft, deflects under the needed clamp.

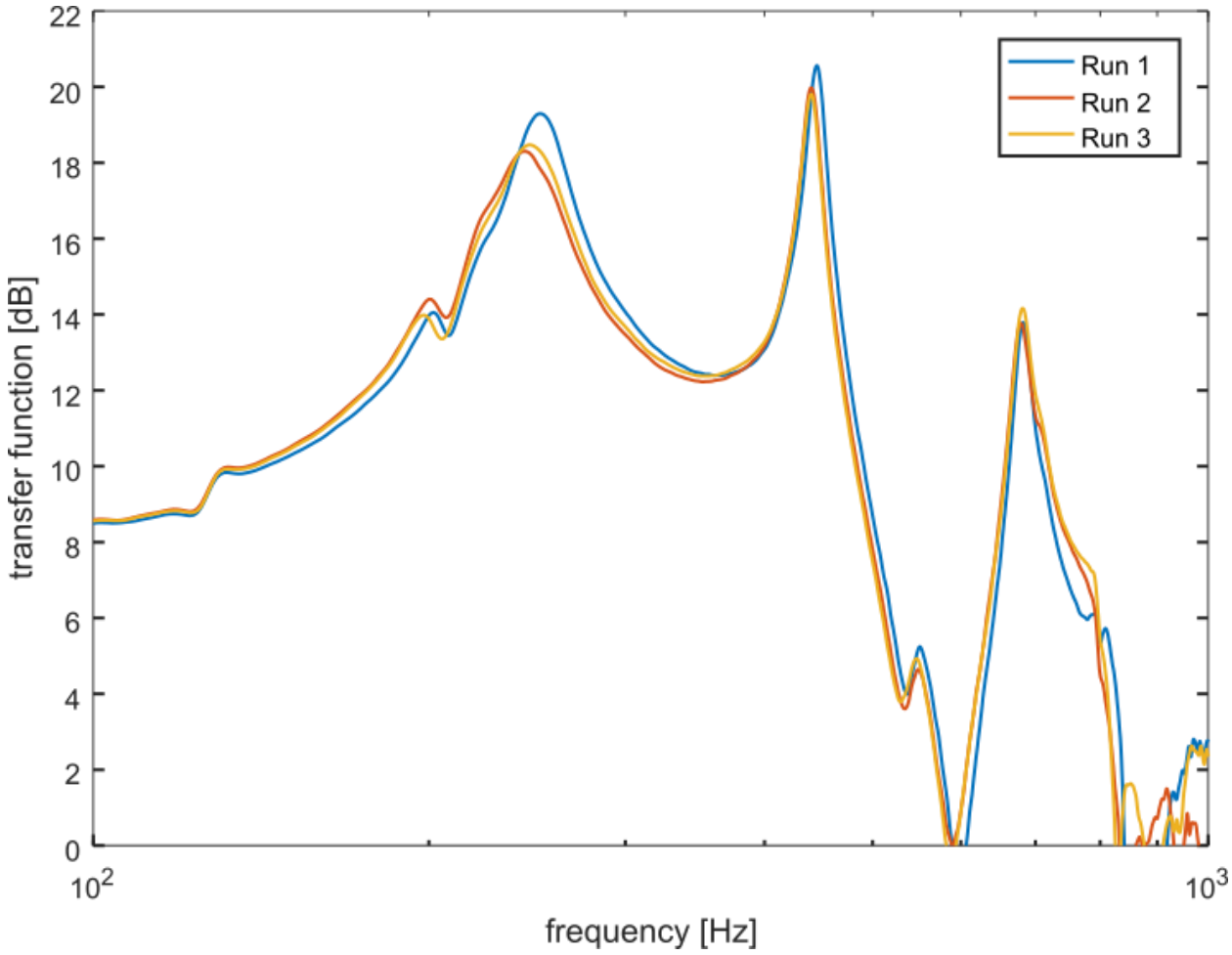

Figure 25. Three experiments are conducted on each specimen to check for consistency in clamping between experiments. This particular plot shows the consistency in experiments for specimen N-V

Experiment results of the frequency response of the specimens are shown in Table 5.

Table 5. FE model and experiment results of the frequency response of the specimens for random excitation experiments for a fixed-free boundary condition

	First Eig. [Hz]		**Second Eig. [Hz]**		**Third Eig. [Hz]**	
Specimen ID	FE Model	Exp.	FE Model	Exp.	FE Model	Exp.
N-V	275	248	375	443	867	679
1-2-3-N	264	246	368	439	845	683
1-2-A	293	224	387	522	817	721
3-A	275	228	378	442	828	694

Table 5 shows large deviation in results for the random excitation experiments for the fixed-free boundary condition panel specimens. Since replicating fixed-free boundary conditions in experiments can be difficult, the FE model is adjusted to a pinned-free boundary condition and, as it was found to be useful in the impact hammer experiments for the free-free boundary condition panels, the mass loading effects of the accelerometers are included in the FE model as well. With the same experimental data, Table 6 shows that the FE model results after boundary condition and mass loading adjustments are much closer to the experimental data.

Table 6. FE model and experimental results of the frequency response of the specimens for random excitation experiments for a pinned-free boundary condition

	First Eig. [Hz]		**Second Eig. [Hz]**		**Third Eig. [Hz]**	
Specimen ID	FE Model	Exp.	FE Model	Exp.	FE Model	Exp.
N-V	248	248	365	443	669	679
1-2-A	242	224	349	522	613	721
3-A	248	228	365	442	694	694
1-2-3-N	238	246	355	439	666	683

Although boundary condition and mass loading adjustments have to be made to the FE model, the random excitation experiments show that the FE model is able to predict the first and third eigenfrequencies of the structural panel specimens. Considering that impact hammer experiments on free-free boundary condition specimens resulted in agreement with FE model results, the random excitation experiments show that correctly replicating FE model boundary conditions in experiments is a challenge. As mentioned in the impact hammer experiments, unaccounted damping and stiffness properties of the voids may be an explanation for deviation between FE modal and experimental results for the voided specimens. In addition, the viscoelastic nature of acrylic makes modeling the specimens as fixed solids unrealistic. The disparities between FE model and experimental results for the second eigenfrequency of the panel specimens may contribute to this explanation when considering the twisting nature of the second mode, as seen in Figure 1, which may lend itself to rocking motion in between the experimental clamps. Despite these uncertainties, the frequency responses of the specimens in Figure 26 show that noticeable changes in eigenfrequencies are achievable with void inclusions.

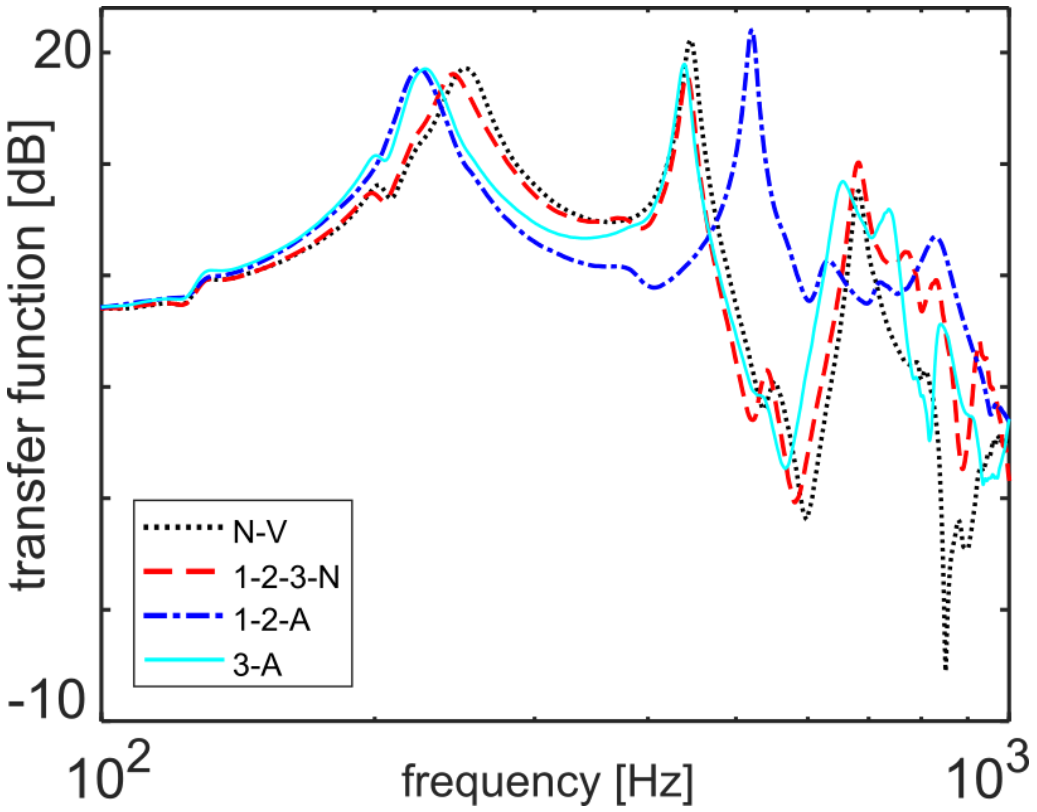

Figure 26. Frequency response of panel specimens from 100-1000 Hz. Individual modes and frequency shifts visible

4 CONCLUSIONS

The ability for a passive or passive-adaptive system to tune its eigenfrequencies away from frequencies associated with external excitation energies has great applicability in situations where a diverse range of dynamic loads are experienced, such as in structural panels of aircraft. In these cases, the lowest order modes of vibration are often the primary cause of undesirable fatigue and are the appropriate modes, and thus eigenfrequencies, to avoid. Research performed on systems with tunable eigenfrequencies has flourished and this concept has been investigated with respect to moveable and adjustable mass and stiffness characteristics, but primarily with nearly one dimensional cantilever beams. The focus on passive vibration control of one dimensional structures has left the capabilities of three dimensional features to accomplish changes in eigenfrequencies unknown.

To begin closing these gaps in knowledge, firstly by finite element modeling, a passive/passive-adaptive structural panel is designed in which the panel can adapt to undesirable frequency input via a transmissible fluid that will pass between strategically placed voids within the panel. Voids, or equivalently mass removal, in areas of higher modal displacement correspond to an increase in eigenfrequency while mass removal in areas of higher stress, or alternatively lower displacement, correspond to a decrease in eigenfrequency. This effect is maximized with larger void sizes and more voids. The FE model suggests that by transferring fluid between strategically placed voids, an eigenfrequency change between positive and negative eigenfrequencies, with respect to those of the panel without voids, is achieved. This yields a 10.0%, 5.0%, and 7.4% change in eigenfrequency for the first, second, and third modes, respectively, of the FE model structural panel.

Then, a sequence of experiments are validation for the FE model predictions. 3-point bend tests are used to more accurately characterize the density and stiffness properties of the cured specimens as compared to the assumed material properties used in FE modeling. Furthermore, the 3-point bend tests verified that curing bubbles that arose out of the fabrication process did not significantly affect the integrity of the specimens. Free-free boundary condition impact hammer experiments validated the FE model for the case of the unvoided specimen and correctly predicted eigenfrequency trends for the voided specimens for all but one eigenfrequency of one specimen. Under random excitation, an attempt is made at recreating the fixed-free boundary condition of the FE model; yet, it is found after experimentation that a pinned-free boundary condition more accurately described the results seen in the finite element model. As seen in the free-free boundary condition experiments, the random excitation results for the first and third eigenfrequencies of the unvoided specimen are accurately captured by the FE model while the voided specimens showed deviation in terms of their trend in eigenfrequency change. Discrepancies in voided specimen experimental results from FE model predictions for both the free-free and pinned-free boundary conditions are potentially

due to an unpredicted result of the void inclusions such as to the bonding layer being a source of stiffness and damping, incomplete internal bonding around their edges, or unknown softening of the areas that the voids are engraved into. Additionally, in the case of the random excitation experiments, the viscoelastic nature of acrylic makes accurately modeling boundary conditions a challenge and the twisting nature of the second mode of the panel specimens may be the cause of discrepancies between experimental and FE model results.

BIBLIOGRAPHY

[1] D. Ewins, "Control of Vibration and Resonance in Aero Engines and Rotating Machinery - an Overview," *International Journal of Pressure Vessels and Piping,* vol. 87, pp. 504-510, 2009.

[2] E. Poursaeidi, A. Babaei, M. Mohammadi Arhani and M. Arablu, "Effects of natural frequencies on the failure of R1 compressor blades," *Engineering Failure Analysis,* vol. 25, pp. 304-315, 2012.

[3] N. Newmark, "Effects of Earthquakes on Dams and Embankments," in *Fifth Rankine Lecture*, London, 1965.

[4] S. Bhaumik, M. Sujata and M. Venkataswamy, "Fatigue Failure of Aircraft Components," *Engineering Failure Analysis,* vol. 15, no. 6, pp. 675-694, 2008.

[5] M. Aykan and M. Celik, "Vibration Fatigue Analysis and Multi-Axial Effect in Testing of Aerospace Structures," *Mechanical Systems and Signal Processing,* vol. 23, no. 3, pp. 897-907, 2009.

[6] L. Librescu, L. Meirovitch and S. Na, "Control of Cantilever Vibration via Structural Tailoring and Adaptive Materials," *American Institute of Aeronautics and Astronautics,* vol. 35, no. 8, pp. 1309-1315, 1997.

[7] A. Baz, K. Imam and J. McCoy, "Active Vibration Control of Flexible Beams using Shape Memory Actuators," *Journal of Sound and Vibration,* vol. 140, no. 3, pp. 437-456, 1990.

[8] K. Alhazza, A. Nayfeh and M. Daqaq, "On Utilizing Delayed Feedback for Active Multi-Mode Vibration Control of Cantilever Beams," *Journal of Sound and Vibration,* vol. 319, pp. 735-752, 2009.

[9] T. Bailey and J. Hubbard, "Distributed Piezoelectric-Polymer Active Vibration Control of a Cantilever Beam," *American Institute of Aeronautics and Astronautics,* vol. 8, no. 5, pp. 605-611, 1985.

[10] Y. Wang, M. Masourni and M. Gaucher-Petitdemange, "Damping Analysis of a Flexible Cantilever Beam Containing an Internal Fluid Channel: Experiment, Modeling and Analysis," *Journal of Sound and Vibration,* vol. 340, pp. 331-342, 2015.

[11] B. Zhu, C. Rahn and C. Bakis, "Fluiduc flexible matrix composite vibration absorber for a cantilever beam," *Journal of Vibration and Acoustics,* vol. 137, p. 021005, 2015.

[12] V. Babitsky and A. Veprik, "Damping of Beam Forced Vibration by a Moving Washer," *Journal of Sound and Vibration,* vol. 166, no. 1, pp. 77-85, 1993.

[13] J. Thomsen, "Vibration Suppression by Using Self-Arranging Mass: Effects of Adding Restoring Force," *Journal of Sound and Vibration,* vol. 197, no. 4, pp. 403-425, 1996.

[14] K. Prakah-Asante and K. Craig, "The Application of Multi-Channel Design Methods for Vibration Control of an Active Structure," *Smart Materials and Structures,* vol. 3, no. 3, pp. 329-343, 1994.

[15] C. Zhang and J. Ou, "Modeling and Dynamical Performance of the Electromagnetic Mass Driver System for Structural Vibration Control," *Engineering Structures,* vol. 82, pp. 93-103, 2015.

[16] G. Ferrari and M. Amabili, "Active Vibration Control of a Sandwich Plate by Non-Collocated Positive Position Feedback," *Journal of Sound and Vibration,* vol. 342, pp. 44-56, 2015.

[17] C. Fuller, S. Snyder, C. Hansen and R. Silcox, "Active Control of Interior Noise in Model Aircraft Fuselages Using Piezoceramic Actuators," *American Institute of Aeronautics and Astronautics,* vol. 30, no. 11, pp. 2613-2617, 1992.

[18] T. Burg, J. Sader and S. Manalis, "Nonmonotonic Energy Dissipation in Microfluidic Resonators," *Physical Review Letters,* vol. 102, no. 22, pp. 1-4, 2009.

[19] Y. Liu, H. Matsuhisa and H. Utsuno, "Semi-Active Vibration Isolation System with Variable Stiffness and Damping Control," *Journal of Sound and Vibration,* vol. 313, no. 1-2, pp. 16-28, 2008.

[20] G. Chen and J. Wu, "Optimal Placement of Multiple Tune Mass Dampers for Seismic Structures," *Journal of Structural Engineering,* vol. 127, no. 9, pp. 1054-1062, 2001.

4 APPENDIX

```
%% data acquisition toolbox NI
clear all
warning off

%%
% preset post-processing built for load-frame experiments using load cell
% and displacement transducers

%% acquire data?
dataacquire=1; % yes for acquire

%% experimental setup parameters
d.test_name='load_frame'; % type of excitation delivered to beam

%% test specimen name, parameters
d.specimen='acrylic_specimen_S_020817_3'; % specimen name, or no_specimen if none

%% data acquisition setup parameters
d.fs=256*1; % sampling frequency [Hz]
d.wind=@hann; % window type for averages
d.seconds=130; % [s] seconds of data acquisition,
d.filter_data_lo=35; % [Hz] of low pass cut off frequency

%% filename for save d structure
c=clock; % grab the time-stamp, eliminates possibility of data overwrite
d.filename=[num2str(c(1))  '_'  num2str(c(2),'%02.0f')  '_'  num2str(c(3),'%02.0f')  '_'
num2str(c(4),'%02.0f')  '_'  num2str(c(5),'%02.0f')  '_'  num2str(c(6),'%02.0f')  '_'
d.test_name '_' d.specimen '.mat'];
saveon=1; % save the data?

%% sensor sensitivity
d.sensor{1}='PCB_110205A_SN920_load_cell_and_signal_conditioner_8162011A_SN1273';
d.ch_sens(1)=110/10; % N/V
d.sensor{2}='Micro_epsilon_ILD1700_SN1503086_laser_displacement_sensor';
d.ch_sens(2)=20/1; % mm/V

%% mean sensor values [V] for each channel, to be subtracted from the input before
sensitivity to [units]
d.data_mean(1)=0.300549698129200; %
d.data_mean(2)=3.468488515621595; %

%% if for data acquisition
if dataacquire==1 % 1=yes for acquire

%% identify connected devices
devices=daq.getDevices;
% once obtained, ensure using correct device name in below session and acquire lines

%% acquire data
s=daq.createSession('ni');
s.addAnalogInputChannel('Dev3',13,'Voltage'); % add input channels
s.addAnalogInputChannel('Dev3',14,'Voltage'); % add input channels
s.Rate=d.fs; % set output and measuring frequency [Hz]
s.DurationInSeconds=d.seconds; % [s] duration of data acquisition
[d.data,d.time_series]=s.startForeground;
d.nn_chan=min(size(d.data));

%% bandpass filter data
```

```
clear ch_f
d.nn_chan=min(size(d.data));
myfilt=designfilt('lowpassiir','filterorder',4,'passbandfrequency',d.filter_data_lo,'P
assbandRipple',0.01,'samplerate',d.fs);
%
myfilt=designfilt('bandpassiir','filterorder',4,'HalfPowerFrequency1',d.filter_data_lo
,'HalfPowerFrequency2',d.filter_data_hi,'samplerate',d.fs);
for iii=1:d.nn_chan
ch_f(:,iii)=filtfilt(myfilt,d.ch_sens(iii)*(d.data(:,iii)-d.data_mean(iii))); %
end

%%
end

%% assign filtered data
d.data_filt=ch_f; % re-assign filtered data from local to structure variable

%% plot
smooth_inc=101;
figure(3);
%clf;
hold on;
trunc=100:30:round(1*length(d.time_series));
% plot(d.data(trunc,2),-d.data(trunc,1))
plot(1e-0*d.data_filt(trunc,2),smooth(-d.data_filt(trunc,1),smooth_inc))
xlabel('displacement [mm]');
ylabel('force [N]');
title([strrep(d.filename,'_','-')])

figure(4);
%clf;
hold on;
% plot(d.data(trunc,2),-d.data(trunc,1))
plot(d.data_filt(trunc,2),1e-3*gradient(smooth(-
d.data_filt(trunc,1),smooth_inc))./gradient(smooth(1e-
3*d.data_filt(trunc,2),smooth_inc)))
xlabel('displacement [mm]');
ylabel('stiffness [kN/m]');
title([strrep(d.filename,'_','-')])

%% save data
if saveon==1
  d.data_filt=[];
  save(d.filename,'d');
end

%%
```